System Simulation of a PMSM Servo Drive Using Field-Circuit Coupling

Thomas Herold, Enno Lange, and Kay Hameyer

Institute of Electrical Machines, RWTH Aachen University, D-52062, Aachen, Germany

In the development process of electrical drive trains, consisting of a motor, the power electronics and the control scheme, it is difficult to predict the exact machine and control behavior in combination with the converter. Therefore, system simulations with analytical machine models embedded in a circuit simulation environment are performed. In order to increase accuracy by paying attention to parasitic machine effects caused by e.g. saturation or slot harmonics, a Finite Element model can be used instead of the analytical machine model. In this paper such a field-circuit coupling is applied to the simulation of a permanent magnet synchronous machine servo drive and the results are shown and discussed.

Index Terms—**Circuit simulation, electromagnetic coupling, finite element methods, permanent magnet machine, simulation.**

I. Introduction

WITHIN the design process of electrical drive trains the system simulation represents an important step. Because servo drives do not only consist of the electrical machine but also of the power electronics and the control, it is necessary to consider all corresponding parts to achieve a proper operation in all working points. Especially for complex control strategies like self-sensing where saturation and inverter influences have to be taken into account this becomes very important [1], [2]. With circuit simulation software it is possible to combine the converter and the control with an analytical representation of the machine. Since the magnetic circuit of the machine is typically designed with the help of Finite Element Analysis (FEA) in order to develop high power, highly efficient, or low noise machines [3]–[5] it is reasonable to take the FE model into consideration, which can substitute the analytical model for a more precise simulation. Especially for machines that operate in magnetic saturation and for those with concentrated windings that do not entirely fulfill the assumption of a sinusoidal winding distribution [6] this simulation method can improve accuracy compared to a dq-model based simulation. In this paper a system simulation of a PMSM servo drive is presented. The used circuit simulator (CS) is PLECS associated with the block diagram oriented simulation environment Matlab/Simulink (AS). For the FEA an IEM in-house software (www.iem.rwth-aachen.de) is applied. After an introduction to the simulated components and the appropriate simulation methods at hand, the system simulation is performed and the results are shown.

II. Simulation Environment

All simulation components are embedded in Simulink, i.e. the machine control, the CS, the FEA, the electrical and mechanical equations together, and the trigger control that forces a new extraction of a set of lumped parameters representing the electrical machine (Fig. 1). The dashed box represents the field-circuit coupling (FCC). In the following the single components are enlarged and the parameter and signal exchange is explained.

Manuscript received May 31, 2010; accepted October 26, 2010. Date of current version April 22, 2011. Corresponding author: T. Herold (e-mail: thomas.herold@iem.rwth-aachen.de).

Digital Object Identifier 10.1109/TMAG.2010.2090866

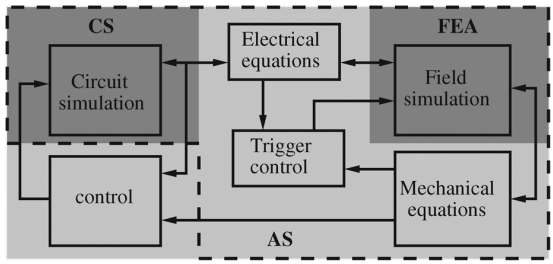

Fig. 1. The overall simulation environment.

A. Lumped Parameter Extraction From FEA

Whenever the trigger control sends a signal, a new set of lumped parameters must be extracted from the FE model. For the device under test, a continuous evaluation of the energy flows of the electrical as well as the mechanical domain ensures a smooth extraction of the parameters [7], which is based on the balance of energy of the electrical machine, as presented in [8]. The three-phase PMSM is represented by an inductance matrix L^{∂}_{kl} of self and mutual inductances with dimension 3×3 and a vector of motion induced voltages e_k with dimension three. The flux induced voltage of phase k is given by the time derivative of the flux linkage ψ_k (with implicit summation over l) as the difference of the terminal voltage v_k and the ohmic voltage drop Ri_k:

$$\partial_t \psi_k = v_k - Ri_k = \partial_t \psi_{kl} + \partial_t \psi_{f,k}. \tag{1}$$

Herein, $\psi_{f,k} = f(\alpha)$ is the remanence flux embraced by the permanent magnets being a function of the angular position of the rotor $\alpha = f(t)$, and $\psi_{kl} = f(\alpha, i_l)$ is the flux linkage in phase k depending on the current $i_l = f(t)$ carried by phase l and the rotor position α. Applying the differential operator in (1) yields:

$$\begin{aligned}
\partial_t \psi_k &= \partial_t (L_{kl} i_l) + \partial_t \psi_{f,k} \\
&= (\partial_t L_{kl}) i_l + L_{kl} (\partial_t i_l) + \partial_t \psi_{f,k} \\
&= (\partial_t i_l \partial_{i_l} L_{kl})\, i_l + \omega (\partial_\alpha L_{kl}) i_l + L_{kl} (\partial_t i_l) + \partial_t \psi_{f,k} \\
&= \partial_t i_l \left((\partial_{i_l} L_{kl})\, i_l + L_{kl} \right) + \omega (\partial_\alpha L_{kl}) i_l + \omega \partial_\alpha \psi_{f,k} \\
&= (\partial_t i_l) L^{\partial}_{kl} + \omega \partial_\alpha \psi_k = (\partial_t i_l) L^{\partial}_{kl} + \omega e^*_k.
\end{aligned} \tag{2}$$

The first term of (2) expresses the induced voltage by the flux linkage described by the inductance matrix L^{∂}_{kl} and the second

term the motion induced voltage with the speed normalized electromotive force (emf) e_k^*.

1) Extraction of the Inductance Matrix: Let

$$M_{ij}(\mathbf{a})a_j = b_i, \tag{3}$$

with the right hand-side (implicit summation over l)

$$b_i = \int_\Omega \mathbf{j}\cdot\boldsymbol{\alpha}_i = i_l \int_\Omega \mathbf{w}_l\cdot\boldsymbol{\alpha}_i := i_l W_{il}, \tag{4}$$

be the nonlinear 2D FE equations describing the PMSM with permanent magnet excitation and stator currents. Herein, $\mathbf{j}$ is the current density and $\boldsymbol{\alpha}_i$ are the shape functions of the degrees of freedom i.e. the nodes. The magnetic vector potential is given by $\mathbf{a}$ and $\mathbf{M}$ is the nonlinear system matrix arising from the Galerkin scheme, see [9]. In 2D, the current shape functions become $\mathbf{w}_k = (w_l/A_l)\mathbf{e}_z$ with w_l being the turns of phase l and A_l the corresponding turn area. Following (4), W_{il} is defined as the current shape vector with respect to phase l.

Now, let i_l^* be the currents at time t, and $b_i^* = i_l^* W_{il}$ the corresponding right-hand sides. Solving (3) with $b_i \equiv b_i^*$ and a fixed rotor angular position $\Delta\alpha = 0$ gives a_j^* and a first order linearization around this particular solution writes

$$M_{ij}\left(a_j^* + \Delta a_j\right) = M_{ij}a_j^* + J_{ij}\Delta a_j = b_i^* + \Delta b_i \tag{5}$$

with the Jacobian matrix $J_{ij} \equiv (\partial_{a_j} M_{in}(a_j^*))a_n^*$. Since $M_{ij}a_j^* = b_i^*$, one has

$$J_{ij}\left(a_j^*\right)\ \Delta a_j|_{\Delta\alpha=0} = \Delta b_i. \tag{6}$$

One can now repeatedly solve (6) with the right-hand sides $\Delta b_i = \Delta i_l\ W_{il}$ obtained by perturbing one after the other m phase currents i_l and obtain m solution vectors for $\Delta a_j|_{\Delta\alpha=0}$. Since (6) is linear, the magnitude of the perturbations Δi_l is arbitrary. One can so define by inspection the inductance matrix L_{kl}^∂ of the electrical machine seen from terminals as

$$\begin{aligned}\Delta\psi_k|_{\Delta\alpha=0} &= W_{kj}\ \Delta a_j|_{\Delta\alpha=0}\\ &= W_{kj}J_{ji}^{-1}\left(a_j^*\right)W_{il}\ \Delta i_l, \equiv L_{kl}^\partial\ \Delta i_l\end{aligned} \tag{7}$$

with

$$L_{kl}^\partial = W_{kj}J_{ji}^{-1}\left(a_j^*\right)W_{il}. \tag{8}$$

2) Extraction of the Motion Induced Voltage: One can now complement (2) to account for the emf:

$$\Delta\psi_k = L_{kl}^\partial\Delta i_l + \omega e_k^* \tag{9}$$

with $e_k^* \equiv \partial_\alpha\psi_k$. The direct computation of the α derivative requires to slightly shift the rotor, remesh, solve the FE problem, evaluate new fluxes and calculate a finite difference. In order to avoid this tedious process, one can again call on the energy principles. One has

$$e_k^* = \partial_\alpha\psi_k = \partial_\alpha\partial_{i_k}\Psi_M = \partial_{i_k}\partial_\alpha\Psi_M = \partial_{i_k}T \tag{10}$$

where T is the torque and Ψ_M is the magnetic energy of the system. During the identification process described above, it is thus easy to calculate additionally the torque corresponding to the perturbed solutions $\Delta\mathbf{a}_j|_{\Delta\alpha=0}$, and to evaluate the motion induced voltage e_k of each phase k as the variation of torque with the perturbation of the corresponding phase current i_k.

Beware however that, as the torque is a nonlinear function of the fields, the perturbations need in this case to be small. Because of the linearity of (6), one may scale the perturbation currents in (10) which yields:

$$e_k^* = \frac{T(\mathbf{a}^*) - T(\mathbf{a}^* + \lambda\Delta\mathbf{a}|_{\Delta\alpha=0})}{\lambda\Delta i_k}\ \text{ with }\ \lambda = \kappa\frac{\|\mathbf{a}^*\|_2}{\|\Delta\mathbf{a}\|_2}. \tag{11}$$

Herein, the scale factor is chosen between $0.01 \le \kappa \le 0.05$.

B. Trigger Control

The trigger control is an important aspect of the field-circuit coupled simulation. Herein, the time step of the FEA is determined. The implemented FCC is based on the weak coupling implying different steps for the circuit simulations and the FEA. This may save a lot of computational effort since the time constant of the field domain τ_{FEA} usually exceeds the time constant of the circuit domain τ_{AS} by orders of magnitude and thus the relation for the time steps is $\Delta T_{FEA} \gg \Delta T_{AS}$. The simplest approach for trigger generation is using a fixed step size. But if e.g. the currents are changing relatively fast, the lumped parameter representation of the machine would change significantly, especially if the machine operates in saturation. On the contrary, if the operating point is not or even slowly changing, an unnecessary, time consuming, extraction of a new set of lumped parameters may be forced.

A more reasonable approach is to adapt the time step. This can be done by energy considerations. Whenever the energy in the system is changing by a certain amount the trigger control enforces an extraction of a new set of lumped parameters from the FEA. The energy in the system is subdivided in four parts, which are calculated as follows (with implicit summation over k).

The electrical energy is given by the terminal values v_k and i_k:

$$E_{elec} = \int v_k i_k \mathrm{d}t. \tag{12}$$

The ohmic losses of the windings have to be considered as well:

$$E_{ohmic} = R\int i_k^2 \mathrm{d}t. \tag{13}$$

The energy

$$E_{mag} = \frac{1}{2}i_k\psi_k = \frac{1}{2}i_k\int\left(v_k - Ri_k - \omega e_k^*\right)\mathrm{d}t \tag{14}$$

represents the magnetic energy stored in the field of the machine's coils. The mechanical energy is calculated by rotational speed and torque:

$$E_{mech} = \int \omega T \mathrm{d}t. \tag{15}$$

A new trigger signal is now generated at the time $t_1 \ge t_0$ of the last valid parameter extraction when the overall energy $E_{tot} = \sum E$ changes by a given specific threshold p, e.g., $p = 5\%$:

$$t_1 = t_0 + \Delta T_{FEA} \tag{16}$$

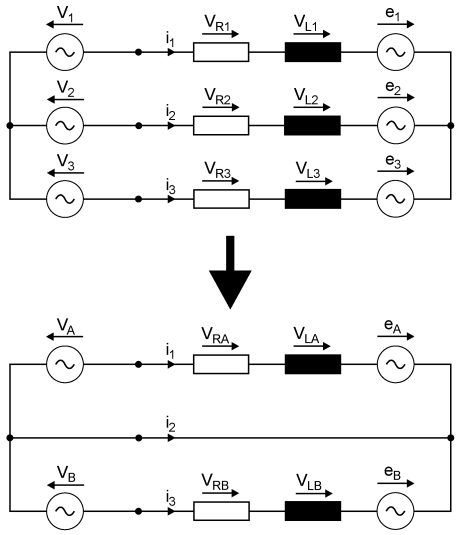

Fig. 2. Reducing of circuit elements to solve overdetermination.

with

$$\Delta T_{FEA} = t|_{(e_{tot} \geq p)} - t_0 \tag{17}$$

and

$$e_{tot} = \frac{E_{tot}(t)}{E_{tot}(t_0)}. \tag{18}$$

To ensure that position dependent influences are not neglected if the energy change remains below p, an additional trigger condition for the position is applied

$$\Delta T_{FEA} = t|_{(\Delta\alpha \geq \alpha_0)} - t_0 \tag{19}$$

where $\Delta\alpha = \alpha(t) - \alpha(t_0)$ is the change of the rotor position and α_0 a predefined difference angle. After a trigger signal has been sent the time t_0 is set to the new time t_1.

C. Electrical and Mechanical Equations

Electrical Equations: The line currents of the machine are calculated by (1) and (2) after being transformed to

$$i_k = \left(L_{kl}^{\partial}\right)^{-1} \int (v_k - Ri_k - \omega e_k^*)\,\mathrm{d}t.$$

Since there is no zero phase-sequence system, the current equation above is overdetermined if solved independently for each phase. To solve this overdetermination the system is transformed as shown in Fig. 2. Now, only two phase currents are calculated whereas the third is given by Kirchhoff's law. This is implemented within the simulation block "Electrical equations." The terminal voltages are provided by the inverter represented within the circuit simulator. The currents are sent back to the circuit simulator and given to the FEA as well.

Mechanical Equations: As aforementioned, the time steps of the FEA and the AS parts are different. Therefore, it is necessary to calculate the speed ω and position angle α of the machine outside the FEA to obtain a smooth curve. This is done by the mechanical equations

$$\omega = \frac{1}{J} \int (T_{el} - T_{load} - T_{loss})\mathrm{d}t, \tag{20}$$

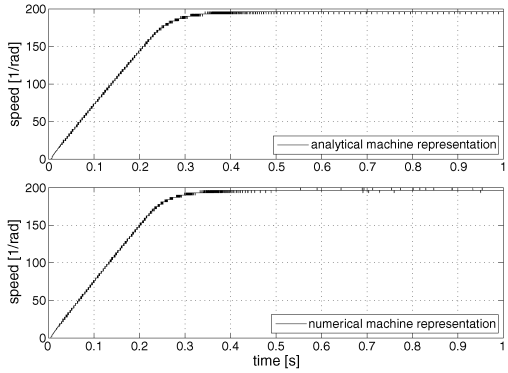

Fig. 3. Startup operation—speed.

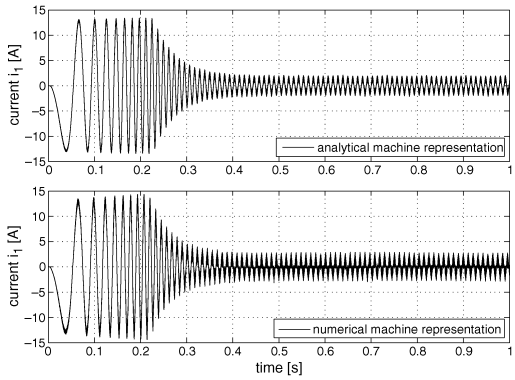

Fig. 4. Startup operation—currents.

$$\alpha = \int \omega \mathrm{d}t \tag{21}$$

where J is the moment of inertia, T_{el} the electrical torque of the machine, T_{load} the machine's load, and T_{loss} the speed dependent losses. The electromagnetic torque is calculated by the FEA which in turn is fed by the phase currents and the rotor position α.

D. Control

Operating a PMSM servo commonly requires a closed loop control. Here, we use a PI cascade with an inner torque and an outer speed control. The duty cycles for the PWM are generated by a space vector modulation [10].

III. Results

For the verification of the described field-circuit coupled simulation approach a system simulation of a PMSM drive train is performed and compared to a simulation with an analytical representation of the machine. The analytical model is fed with data sheet parameters whereas the FCC gets the machine parameters by the lumped parameter extraction introduced in chapter II-A.

For the test condition a startup operation with no load (except friction) is simulated and the speed ω and the phase current i_1 of the analytical machine representation is opposed to these of the numerical machine representation (Fig. 3 and 4).

It can be seen that there are only minor deviations between the two simulation approaches. In the current plots a higher noise is observable. This is because of the saturation effects of the machine material which are not considered in the analytical machine representation. A closer look on these effects is given by

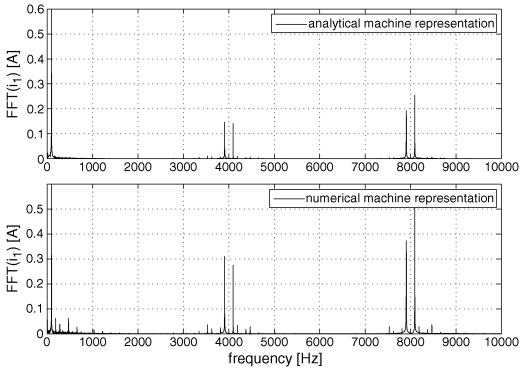

Fig. 5. Startup operation—FFT analysis of currents.

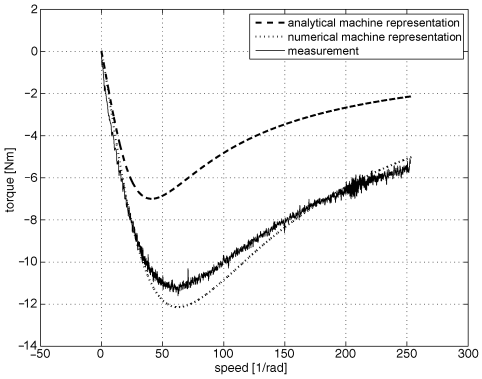

Fig. 6. Torque vs. current at short circuit operation (comparison).

the FFT of the steady state currents $(t = 0.5 \ldots 1.0\,\mathrm{s})$ is given in Fig. 5. The influence of the PWM supply is clearly visible at 4 and 8 kHz. Here, the current amplitude of the FCC simulation is double the amplitude of the analytical simulation. This emphasizes the saturation effect that results in lower inductances than given in the data sheet. Furthermore, cogging and slotting effects are reflected in the frequency range below 1000 Hz that are omitted in the idealized analytical simulation. Another conducted experiment is the short circuit operation that blinds out the effects of the control and the inverter driven voltages. In Fig. 6 the machine torque vs. the speed is plotted. Additional to the two simulation methods a measurement is given as well. The analytical simulation gives a maximum breaking torque of approx. 7 Nm whereas the numerical simulation shows over 12 Nm. This bases again on the saturation, since the short-circuit current is higher at a smaller reactance. Compared to the analytical simulation the numerical simulation shows a good correlation to the measurement. Nevertheless, there are some deviations that call for further investigations.

IV. Conclusion

This paper presents the system simulation of an electrical drive train by means of a field-circuit coupled approach and explains the basic principles. Within the simulations an FE model of a PMSM is combined with a circuit simulation tool. This approach considers nonlinearities, saturation effects, mutual magnetization influences of the d- and q-axis, etc., whose inclusion in analytical models is hardly to accomplish. By means of a start-up simulation the numerical representation is compared to an analytical representation of the machine. A short-circuit operation is simulated as well and compared to a measurement.

The experiments show promising results with regard to improvement of simulation accuracy. In future works the method will be further evaluated by comprehensive simulations and measurements. The influence of material properties as well as the capabilities for loss calculation or fault simulation will be investigated. Furthermore, tolerance in the machine construction (unbalanced magnetization, eccentricities, ...) that result in asymmetrical behavior will be analyzed.

References

[1] D. D. Reigosa, P. Garcia, D. Raca, F. Briz, and R. D. Lorenz, "Measurement and adaptive decoupling of cross-saturation effects and secondary saliencies in sensorless controlled IPM synchronous machines," *IEEE Trans. Ind. Appl.*, vol. 44, no. 6, pp. 1758–1767, Nov./Dec. 2008.

[2] Y. Li, Z. Q. Zhu, D. Howe, and C. M. Bingham, "Modeling of cross-coupling magnetic saturation in signal-injection-based sensorless control of permanent-magnet brushless AC motors," *IEEE Trans. Magn.*, vol. 43, no. 6, pp. 2552–2554, Jun. 2007.

[3] C. Zhao, H. Qin, and Y. Yan, "Analysis of the pole numbers on flux and power density of IPM synchronous machine," in *Proc. PEDS*, 2005, vol. 2, pp. 1402–1407.

[4] M. C. Tsai, M. H. Weng, and M. F. Hsieh, "Computer-aided design and analysis of new fan motors," *IEEE Trans. Magn.*, vol. 38, no. 5, pp. 3467–3474, Sep. 2002.

[5] D. Franck and K. Hameyer, "Simulation of acoustic radiation of an AC servo drive verified by measurements," in *Proc. ISEF*, 2009.

[6] A. M. El-Refaie and T. M. Jahns, "Optimal flux weakening in surface PM machines using fractional-slot concentrated windingsg," *IEEE Trans. Ind. Appl.*, vol. 41, no. 3, pp. 790–800, May/Jun. 2005.

[7] E. Lange, F. Henrotte, and K. Hameyer, "An efficient field-circuit coupling based on a temporary linearization of FE electrical machine models," *IEEE Trans. Magn.*, vol. 45, no. 3, pp. 1258–1261, Mar. 2009.

[8] F. Henrotte and K. Hameyer, "The structure of EM energy flows in continuous media," *IEEE Trans. Magn.*, vol. 42, no. 4, pp. 903–906, Apr. 2006.

[9] J. P. A. Bastos and N. Sadowski, *Electromagnetic Modeling by Finite Element Methods*. New York: Marcel Dekker, 2003.

[10] H. W. van der Broeck, H.-C. Skudelny, and G. V. Stanke, "Analysis and realization of a pulsewidth modulator based on voltage space vectors," *IEEE Trans. Ind. Appl.*, vol. 24, no. 1, pp. 142–150, Jan./Feb. 1988.